Synthesis and Evaluation of ^{11}C-LY2795050 as a κ-Opioid Receptor Antagonist Radiotracer for PET Imaging

Ming-Qiang Zheng[1], Nabeel Nabulsi[1], Su Jin Kim[1], Giampaolo Tomasi[1], Shu-fei Lin[1], Charles Mitch[2], Steven Quimby[2], Vanessa Barth[2], Karen Rash[2], John Masters[2], Antonio Navarro[2], Eric Seest[2], Evan D. Morris[1], Richard E. Carson[1], and Yiyun Huang[1]

[1]*PET Center, Department of Diagnostic Radiology, Yale University, New Haven, Connecticut; and* [2]*Eli Lilly and Co., Indianapolis, Indiana*

Kappa-opioid receptors (KOR) are believed to be involved in the pathophysiology of depression, anxiety disorders, drug abuse, and alcoholism. To date, only 1 tracer, the KOR agonist ^{11}C-GR103545, has been reported to be able to image KOR in primates. The goal of the present study was to synthesize the selective KOR antagonist ^{11}C-LY2795050 and evaluate its potential as a PET tracer to image KOR in vivo. **Methods:** The in vitro binding affinity of LY2795050 was measured in radioligand competition binding assays. Ex vivo experiments were conducted using microdosing of the unlabeled ligand in Sprague–Dawley rats and in wild-type and KOR knockout mice, to assess the ligand's potential as a tracer candidate. Imaging experiments with ^{11}C-LY2795050 in monkeys were performed on the Focus-220 scanner with arterial blood input function measurement. Binding parameters were determined with kinetic modeling analysis. **Results:** LY2795050 displays full antagonist activity and high binding affinity and selectivity for KOR. Microdosing studies in rodents and ex vivo analysis of tissue concentrations with liquid chromatography–tandem mass spectrometry identified LY2795050 as an appropriate tracer candidate able to provide specific binding signals in vivo. ^{11}C-LY2795050 was prepared in an average yield of 12% and greater than 99% radiochemical purity. In rhesus monkeys, ^{11}C-LY2795050 displayed a moderate rate of peripheral metabolism, with approximately 40% of parent compound remaining at 30 min after injection. In the brain, ^{11}C-LY2795050 displayed fast uptake kinetics (regional activity peak times of $<$20 min) and an uptake pattern consistent with the distribution of KOR in primates. Pretreatment with naloxone (1 mg/kg, intravenously) resulted in a uniform distribution of radioactivity. Further, specific binding of ^{11}C-LY2795050 was reduced by the selective KOR antagonist LY2456302 in a dose-dependent manner. **Conclusion:** ^{11}C-LY2795050 displayed favorable pharmacokinetic properties and binding profiles in vivo and therefore is a suitable ligand for imaging the KOR in primates. This newly developed KOR antagonist tracer has since been advanced to PET imaging of KOR in humans and constitutes the first successful KOR antagonist radiotracer.

Key Words: kappa opioid receptor; antagonist; PET; radioligand; synthesis

J Nucl Med 2013; 54:455–463
DOI: 10.2967/jnumed.112.109512

The opioid receptors belong to the superfamily of G-protein–coupled receptors and are generally classified into at least 3 subtypes: δ-opioid receptors (DOR), κ-opioid receptors (KOR), and μ-opioid receptors (MOR) (*1*). The opioid receptors share extensive homology (*2*) but differ both in their pharmacology and in their physiologic effects. Agonists at the MOR and DOR sites are rewarding and reinforcing, and agonists at the KOR sites are aversive.

The distribution of opioid receptors has been established using autoradiographic methods. In rodents, MOR was found to be most dense in the cingulate cortex, amygdala, hippocampus, nucleus accumbens, striatum, thalamus, and raphe nuclei (*3–5*). DOR is distributed in more limited areas, such as the cingulate cortex, amygdala, nucleus accumbens, and striatum (*3–5*). KOR is less widespread than MOR in the rodent brain and is densely distributed in the amygdala, nucleus accumbens, striatum, and thalamus (*4,6,7*).

The distribution of KOR in the human brain differs in some important ways from that in the rodent brain. KOR binding in the human brain is widespread and is found in greater density than MOR throughout the central nervous system in most cortical and subcortical regions (*8–10*). KORs and messenger RNA are present in the deep layers of cortical brain regions, including the frontal and temporal cortices, and in the striatum, hippocampus, amygdala, thalamus, and cerebellum (*8,10,11*). A similar distribution of KOR is seen in the nonhuman primate brain (*12,13*).

KOR is present in several structures of the human brain thought to be critical in mood modulation, perception, learning, memory, and behavior response to drugs of abuse. Thus, KOR plays an important role in the regulation of brain functions and is involved in a variety of neurologic and psychiatric diseases, addictive disorders, and other diseases of the brain such as depression, anxiety, cocaine

Received Jun. 16, 2012; revision accepted Sep. 18, 2012.
For correspondence or reprints contact: Yiyun (Henry) Huang, PET Center, Department of Diagnostic Radiology, Yale University School of Medicine, P.O. Box 208048, 801 Howard Ave., New Haven, CT 06520-8048.
E-mail: henry.huang@yale.edu
Published online Jan. 25, 2013.

dependence, alcoholism, and Alzheimer's disease (*14*). Hence, KOR is a target for the development of drugs to treat depression, anxiety, drug abuse, and alcoholism. As such, the successful development and application of selective PET radiotracers for KOR imaging in humans will allow the investigation of its involvement in neuropsychiatric and addictive disorders. It will also greatly help the development of novel therapeutic agents by correlating dose, in vivo pharmacokinetic parameters, and receptor occupancy of novel KOR-targeting drugs.

Several opioid receptor radiotracers are currently available for PET in humans, including ^{11}C-carfentanil, ^{11}C- and ^{18}F-diprenorphine, ^{11}C-buprenorphine, ^{18}F-cyclofoxy, and ^{11}C-methylnaltrindole (*15*). However, none of these are selective for KOR.

Attempts have been made to develop KOR-selective radiotracers. The compounds that have been radiolabeled include the κ-agonist U50488 and its fluoroalkyl derivative (*16,17*), GR89696 (**1**, Fig. 1), and GR103545 (**2**, Fig. 1) (*18,19*). These ligands are all agonists, and only ^{11}C-GR103545 has been evaluated extensively in nonhuman primates (*20*) and most recently in humans in our laboratory (*21*). Given that KOR agonists possess dysphoric and sedative effects, and induce psychosis at higher doses, the routine use of agonist ligands such as ^{11}C-GR103545 in humans requires strict control of injected mass and hence the synthesis of the radioligand with high specific activity. We and others have recently developed methods for the synthesis of ^{11}C-GR103545 with high yield and high specific activity (*22–24*), which made it possible to perform KOR imaging studies in humans. Nonetheless, tracer mass still requires strict control to prevent the manifestation of KOR agonist effects. On the other hand, application of KOR antagonist radiotracers will have a much wider safety margin, because opioid antagonists such as naloxone and naltrexone have long been used safely in the clinics. For KOR antagonist tracers, ^{11}C-MeJDTic (**3**, Fig. 1) was evaluated in rodents, but no report of its evaluation in higher species is available (*25*). We have recently reported the discovery of a series of aminobenzyloxyarylamides as KOR selective antagonists, including LY2456302 (**4**) and LY2795050 (**5**) (Fig. 1) (*26*). In a preliminary evaluation in rats using tracerlike dose and liquid chromatography–tandem mass spectrometry (LC/MS/MS) determination of ligand tissue concentrations, it was demonstrated that the ligand LY2795050 provides specific binding similar to that of GR103545 and can be used to measure dose-dependent receptor occupancy by a selective KOR antagonist (*26*). From these initial results, we concluded that LY2795050 is a suitable candidate for development as an in vivo imaging agent. In this paper, we report the synthesis of ^{11}C-LY2795050 and its evaluation as the first ever, to our knowledge, antagonist radioligand suitable for imaging KOR in the primate brain.

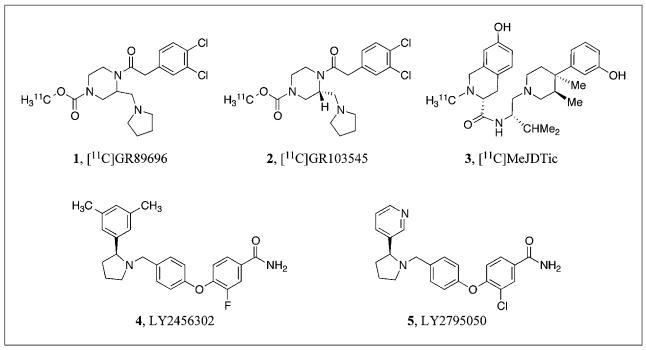

FIGURE 1. Representative KOR ligands.

MATERIALS AND METHODS

Chemistry

All reagents and anhydrous solvents were obtained from commercial sources and used without further purification unless noted otherwise.

^{1}H nuclear magnetic resonance (NMR) spectra were recorded on a Varian 300- or 400-MHz spectrometer. Chemical shifts are reported in parts per million, with the solvent resonance as the internal standard ($CDCl_3$: 7.26 ppm; dimethylsulfoxide [DMSO]-d_6: 2.49 ppm). Optical rotations were measured with a Perkin-Elmer 341 polarimeter.

4-(2-Chloro-4-Iodophenoxy)Benzaldehyde (8). To a solution of 4-fluorobenzaldehyde (**6**) (55.7 g, 449.1 mmol) and **8** (120.0 g, 471.6 mmol) in DMSO (2,000 mL) was added 40% KF on Al_2O_3 (91.3 g, 628.7 mmol) and 18-crown-6 (11.8 g, 44.9 mmol). The mixture was heated at 110°C under nitrogen for 48 h and then cooled to room temperature, whereupon EtOAC (5.0 L) and water (5.0 L) were added and the mixture was filtered. The organic phase in the filtrate was separated and washed with water (2 × 5.0 L). The combined aqueous phase was back-extracted with EtOAC (4.0 L). The combined organic phases were washed successively with water (8.0 L) and brine (4.0 L), dried over $MgSO_4$, filtered, and concentrated under reduced pressure. The resulting crude product was purified by flash chromatography on silica gel eluting with 0%–30% EtOAc in hexanes to afford **8** (102 g, 60%) as light yellow oil. ^{1}H NMR (400 MHz, $CDCl_3$): 9.92 (s, 1H), 7.85 (m, 3H), 7.61 (d, J = 8.4 Hz, 1H), 7.21 (m, 1H), 7.01–6.99 (m, 2H), 6.86 (m, 1H).

3-(1-(4-(2-Chloro-4-Iodophenoxy)Benzyl)Pyrrolidin-2-yl)Pyridine (9). To a solution of **8** (8.50 g, 23.7 mmol) and (±)-nornicotine (3.51 g, 23.7 mmol) in CH_2Cl_2 (300 mL) was added HOAc (2.0 mL, 35.6 mmol) at room temperature. The solution was stirred for 10 min, whereupon $NaBH(OAc)_3$ (7.55 g, 35.6 mmol) was added, and the resulting mixture was stirred at room temperature for 14 h. Saturated aqueous $NaHCO_3$ was added to the reaction mixture to adjust the pH to 8. The mixture was then extracted with CH_2Cl_2 (2 × 200 mL). The combined organic phases were dried over $MgSO_4$, filtered, and concentrated under reduced pressure. The resulting crude product was purified by flash chromatography on silica gel eluting with 0%–100% EtOAc in hexanes to afford **9** (7.6 g, 66%) as a colorless oil. ^{1}H NMR (300 MHz, DMSO-d_6): 8.58 (d, J = 1.5 Hz, 1H), 8.47 (dd, J_1 = 4.8 Hz, J_2 = 1.5 Hz, 1H), 7.82 (dt, J_1 = 7.5 Hz, J_2 = 1.5 Hz, 1H), 7.66 (dd, J_1 = 8.7 Hz, J_2 = 1.8 Hz, 1H), 7.36 (dd, J_1 = 8.0 Hz, J_2 = 4.5 Hz, 1H), 7.24 (d, J = 8.7 Hz, 2H), 6.91 (d, J = 8.7 Hz, 1H), 3.60 (d, J = 13.2 Hz, 1H), 3.46 (t, J = 8.1 Hz, 1H), 3.15 (d, J = 13.2 Hz, 1H), 3.00 (td, J_1 = 6.6 Hz, J_2 = 3.0 Hz, 1H), 2.22 (m, 2H), 1.80 (m, 2H), 1.61 (m, 1H).

(S)-3-(1-(4-(2-Chloro-4-Iodophenoxy)Benzyl)Pyrrolidin-2-yl) Pyridine (10) and (S)-3-(1-(4-(2-Chloro-4-Iodophenoxy)Benzyl) Pyrrolidin-2-yl)Pyridine Hydrochloride Salt (10 • HCl). Racemic compound **9** (18.7 g) was dissolved in MeOH (100 mL) and resolved by supercritical fluid chromatography using a preparative Chiralcel OJ-H column (30 × 250 mm, 5 μm; Chiral Technologies) eluting with 25% MeOH (containing 0.1% diethylamine) in supercritical CO_2 at a flow rate of 80 mL/min. (*S*)-3-(1-(4-(2-chloro-4-iodophenoxy)benzyl)pyrrolidin-2-yl)pyridine **(10)** was isolated as the second eluting peak to give the desired enantiomer (7.85 g, 42%) as a yellow oil.

Compound **10** (7.7 g, 15.8 mmol) was dissolved in EtOAc (748.8 mL) and stirred at room temperature, whereupon 2 M HCl in EtOAc (39.5 mL) was added dropwise to the solution. The mixture was left standing for 25 min. The upper clear layer was separated, concentrated under reduced pressure, and dried under vacuum to give the HCl salt (8.3 g, 100%) as a white solid. Enantiomeric purity was greater than 99% as determined by chiral high-performance liquid chromatography (HPLC) analysis. $[\alpha]_D^{20} = -1.99°$ (*c* 1.0, EtOH). ^{1}H NMR (400 MHz; DMSO-d_6): δ 11.82–11.69 (m, 1H), 8.88 (s, 1H), 8.73 (d, J = 5.3 Hz, 1H), 8.51 (d, J = 7.5 Hz, 1H), 7.96 (t, J = 2.0 Hz, 1H), 7.74–7.69 (m, 2H), 7.59–7.43 (m, 2H), 7.00–6.77 (m, 3H), 4.71–4.67 (m, 1H), 4.37–4.21 (m, 2H), 3.71–3.50 (m, 1H), 3.45–3.16 (m, 1H), 2.34–2.02 (m, 3H).

In Vitro Binding Assays

In vitro binding experiments and GTP-γ-S antagonist functional assays were performed according to the published procedures (*26*).

Ex Vivo Experiments in Rodents

Experiments in rodents were performed under protocols approved by the Animal Care and Use Committee of Eli Lilly and Co.

Male Sprague–Dawley rats weighing 230–280 g were used. κ-knockout (KO) mice were generated on a 129S6 inbred background strain with an exon 3 deletion in accordance with literature procedures (*27–29*).

LY2795050 (1 mg) was dissolved in 1 mL of saline. This initial solution was then diluted to a final concentration of 3 μg/mL and administered in a volume of 1 mL/kg via the lateral tail vein to groups of rats (n = 4 rats in each group) and KOR KO (n = 8) or wild-type (WT) mice (n = 9). Rats were sacrificed at 10, 20, 40, or 60 min after dosing, and mice were sacrificed at 60 min after dosing. The striatum and cerebellum were dissected, weighed, and placed in conical centrifuge tubes cooled on ice. Four volumes (w/v) of acetonitrile containing 0.1% formic acid were added to each tube. Samples were then homogenized using an ultrasonic probe and centrifuged at 14,000 RPM for 16 min. The supernatant was separated and diluted 1 to 9 with sterile water for LC/MS/MS analysis using an HPLC device (model 1200; Agilent Technologies) and an API 4000 mass spectrometer (Applied Biosystems). The chromatographic separation used a C18 column (2.1 × 50 mm; part no. 971700-907 [Agilent]) and a mobile phase consisting of 22% acetonitrile with an overall 0.1% formic acid content. LY2795050 was detected by monitoring the precursor-to-product ion transition with a mass-to-charge ratio (m/z) of 408.3 to 259.9. Standards were prepared by adding known quantities of analyte to brain tissue samples from nontreated rats and processed as described above.

The concentration of LY2795050 in the striatum is presumed to represent total binding, whereas levels in the cerebellum represent nonspecific binding because this is a region with little or no expression of KORs, DORs, and MORs (*30*). The concentration ratio between striatum and cerebellum is presented as a measure of specific binding.

Radiochemistry

The following instruments were used in the radiochemistry procedures: a semipreparative HPLC system including a Shimadzu AT HPLC pump, a Rheodyne 7133i injector with a 2-mL loop, a Genesis C18 column (10 × 250 mm, 4 μm), a Knauer K200 ultraviolet detector with 254-nm wavelength, a Bioscan γ-flow detector, a laptop computer running EZ Start software for system control, an analytic HPLC system consisting of a Shimadzu AT quarternary HPLC pump, a Rheodyne 7133i injector, a Genesis C18 column (4.6 × 250 mm, 4 μm), a Shimadzu SIL PDA detector, a Bioscan Flow Cell γ-detector, and a computer with Shimadzu Class VP software used for system control.

The cyclotron-produced ^{11}C-CO_2 was reacted with hydrogen at 400°C under a nickel catalyst to afford ^{11}C-CH_4, which was converted to ^{11}C-cyanide by reaction with ammonia over a platinum catalyst at 950°C. Radiolabeling was performed by trapping the ^{11}C-cyanide in a solution of the precursor **10** (0.5–3 mg), K_2CO_3, and Pd_2dba_3 in dimethylformamide (0.3 mL) and then reacted at 80°C for 5 min to produce the intermediate ^{11}C-**12**, which then underwent hydrolysis with NaOH (1N, 0.2 mL) and H_2O_2 (0.2 mL) to afford the final product, ^{11}C-LY2795050 (**^{11}C-5**).

Purification of the labeled product, ^{11}C-LY2795050, was achieved by semipreparative HPLC. The column was eluted with 25% MeCN and 75% 0.1 M ammonium formate solution with 0.5% HOAc, at a flow rate of 5 mL/min. The desired product fraction (eluting at 12–14 min) was collected, diluted with water (50 mL), and passed through a C-18 SepPak cartridge (Waters). The SepPak was rinsed with 0.01N HCl (10 mL). The radioactive product, trapped on the SepPak, was recovered by elution with 1 mL of U.S. Pharmacopeial Convention (USP) absolute ethanol, followed by 3 mL of USP saline, into a product vial containing 7 mL of USP saline and 40 μL of 4.2% USP Na_2CO_3 solution. This mixture was then passed through a sterile membrane filter (0.22 μm) and collected in an empty sterile vial to afford a formulated solution ready for injection.

Quality control of the final product was performed by analytic HPLC with a mobile phase of 25% MeCN and 75% 0.1 M ammonium formate with 0.5% acetic acid at a flow rate of 2 mL/min.

The radiochemical purity of the final product was greater than 99%. Identity was confirmed by coinjection of the product with LY2795050 onto the analytic HPLC system and detection of a single ultraviolet peak on the chromatogram (retention time, 6.7 min). Chiral HPLC analysis of the final product indicated that only 1 enantiomer was produced.

PET Experiments in Rhesus Monkeys

PET Procedures. Experiments were performed on 3 rhesus monkeys according to a protocol approved by the Yale University Institutional Animal Care and Use Committee and described previously (*31*). The animals were immobilized with ketamine (10 mg/kg intramuscularly) and anesthetized with 1%–2% isoflurane. For each monkey, an indwelling port was surgically placed in a femoral artery for arterial blood sampling. PET was performed on a Focus 220 scanner (Siemens Medical Solutions). Before radiotracer injection, a 10-min transmission scan was obtained for attenuation correction. The radiotracer was administered by an

infusion pump over 1 min. Emission data were collected in list mode for 120 min and reformatted into 33 successive frames of increasing duration (6 × 10 s, 3 × 1 min, 2 × 2 min, and 22 × 5 min).

Arterial Input Function Measurement and Metabolite Analysis. Procedures associated with measurement of the input function have previously been described (*31*). Briefly, arterial samples were collected at preselected times to measure the radioactivity concentration in plasma and whole blood over time. Five samples, collected at 4, 12, 30, 60, and 90 min after tracer injection, were processed and analyzed by HPLC using a column-switching method of Hilton et al. (*32*). Blood samples in ethylenediaminetetraacetic acid tubes were centrifuged at 2,300*g* at 4°C for 5 min to separate the plasma. Plasma samples were then treated with urea (8 M) and loaded onto a capture column (19 × 4.6 mm) packed with Phenomenex SPE C18 Strata-X sorbent and eluted with 1% acetonitrile in water at a flow rate of 2 mL/min for 4 min, after which the activity trapped on the capture column was backwashed onto a Phenomenex Gemini-NX C18 column (5 μm, 4.6 × 250 mm) eluted with 40% acetonitrile and 60% 0.1 M ammonium formate (v/v) at a flow rate of 1.5 mL/min. HPLC effluent was collected by an automated fraction collector (model CF-1; Spectrum Chromatography), and the fractions were counted in a γ-counter (Wizard^2; Perkin-Elmer). The unmetabolized parent fraction was determined as the ratio of the sum of radioactivity in fractions containing the parent tracer to the total amount of radioactivity collected.

A biexponential function was fitted to the 5 measured parent fractions to provide a continuous function to describe the parent fraction. The input function was then calculated as the product of total counts in the plasma and interpolated parent fraction at each time point. The measured input function values were fitted to a sum of 3 exponentials, and the fitted values were used as inputs for the kinetic analyses.

The plasma-free fraction (f_p) was determined by ultrafiltration (performed in triplicate) of 0.2-mL aliquots of plasma spiked with the radiotracer. The amount of radioactivity in the filter unit and the filtrate was counted. The value of f_p was calculated as the ratio of the concentration (radioactivity/mL) of the filtrate to that of the total.

Image Analysis. PET emission data were attenuation-corrected using the transmission scan, and dynamic images (33 frames over 120 min) were reconstructed using a filtered backprojection algorithm with a Shepp–Logan filter. Regions of interest (ROIs) were delineated on a single representative anatomic rhesus MR image registered to a template image. Registration parameters were obtained to apply ROIs to individual PET scans, and time–activity curves were generated in 15 cortical and subcortical brain regions.

Derivation of Distribution Volume (V_T). Regional total V_T (mL · cm^{-3}) was derived by kinetic analysis of the time–activity curves, using the metabolite-corrected arterial plasma concentrations as the input function, according to a 1-tissue- or 2-tissue-compartment model (1TC or 2TC, respectively). Kinetic parameters (K_1 and k_2 for 1TC; K_1–k_4 for 2TC) were derived first in modeling analysis. In 1TC, K_1 (mL·min·cm^{-3}) and k_2 (min^{-1}) are the rate constants for the transfer of ligand into and out of the brain, respectively. In 2TC, K_1 and k_2 are the rate constants for the transfer of ligand into and out of the nondisplaceable compartment (free and nonspecific binding), whereas k_3 (min^{-1}) and k_4 (min^{-1}) describe the respective rates of association to and dissociation from the receptors.

V_T was derived from kinetic parameters as K_1/k_2 in 1TC and as K_1/k_2 $(1 + k_3/k_4)$ in 2TC (*33*).

The Akaike information criterion and χ^2 were calculated to evaluate the optimal model for derivation of regional V_T.

Derivation of Receptor-Binding Parameters. Cerebellar V_T ($V_{T\ CER}$) was used as an estimate of the nondisplaceable distribution volume in the ROIs. The main outcome measure of interest was the nondisplaceable binding potential (BP_{ND}), calculated as $(V_{T\ ROI} - V_{T\ CER})/V_{T\ CER}$ with the physiologic interpretation of $f_{ND} \times B_{avail}/K_D$, where $V_{T\ ROI}$ is the distribution volume in the region of interest, B_{avail} is the concentration of available binding sites (nmol·cm^{-3} of tissue), K_D is the in vivo equilibrium dissociation constant of the radiotracer (nmol·cm^{-3}), and f_{ND} is the free fraction in the nonspecific pool of the brain ($f_{ND} = f_P/V_{T\ CER}$) (*33*). The simplified reference tissue model (SRTM) was also used to calculate regional BP_{ND} using the cerebellum as the reference region (*34*).

KOR occupancy was calculated using V_T values from multiple brain regions (amygdala, brain stem, caudate, cerebellum, cingulated cortex, frontal cortex, occipital cortex, temporal cortex, globus pallidus, hippocampus, insula, nucleus accumbens, pons, putamen, substantia nigra, and thalamus) to create occupancy plots according to the method of Cunningham et al. (*35*).

RESULTS

Chemistry

The synthesis of compound LY2795050 (**5**), its opposite (*R*)-enantiomer, and the racemic form was described previously (*26*). The preparation of the precursor **10** for the radiosynthesis of ^{11}C-LY2795050 is depicted in Figure 2. 4-Fluorobenzaldehyde (**6**) was coupled with compound **7** to give **8** in 60% yield. Reductive amination with (±)-nornicotine gave rise to compound **9** in 66% yield. The 2 enantiomers were separated by preparative chiral HPLC. The desired (*S*)-enantiomer (**10**) was obtained in greater than 99% chemical purity and greater than 99% enantiomeric purity, as indicated by chiral HPLC analysis (Fig. 3, top).

In Vitro Binding Assays and Ex Vivo Evaluation

Table 1 lists the in vitro binding affinities and functional activities of LY2795050 for opioid receptors, along with those of naltrexone, MeJDTic, and GR103545. LY2795050 displays high affinity (K_i, 0.72 nM) for KOR and over 35-fold selectivity for KOR over other opioid receptors. In functional assays, LY2795050 displays the property of being a full antagonist at all 3 opioid receptors. Given this favorable in vitro profile, ex vivo evaluation was performed to characterize its binding in the rodent brain and assess its potential as a PET tracer candidate using a methodology pioneered at Eli Lilly (*36,37*).

As shown in Figure 4 (left), intravenous administration of LY2795050 (3 μg/kg) to rats led to rapid brain uptake, followed by a relatively fast washout. LY2795050 differentially distributed toward the striatum relative to the cerebellum at all time points. Total binding, as represented by ligand concentration in the striatum, was significantly different from nonspecific binding (i.e., ligand concentration in the cerebellum), resulting in a striatum-to-cerebellum ratio of greater than 2 at 10, 20, and 40 min after injection and 3.3 at 60 min after injection.

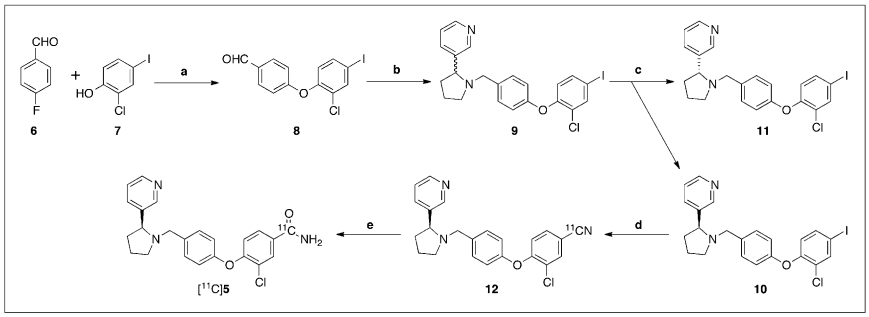

FIGURE 2. Synthesis of radiolabeling precursor (**10**) and ^{11}C-LY2795050 (^{11}C-**5**). Reagents and conditions: a. KF/Al_2O_3, 18-crown-6, DMSO, 110°C; b. (±)-nornicotine, $NaBH(OAc)_3$, HOAc, $ClCH_2CH_2Cl$, rt; c. chiral HPLC; d. H^{11}CN, $KHCO_3$, dppf, Pd_2dba_3, 80°C, 5 min; e. NaOH, H_2O_2, dimethylformamide, 80°C, 5 min.

Binding of LY 2795050 was also assessed in the striatum and cerebellum of WT and KOR KO mice after intravenous dosing of 3 μg/kg. The KOR-specific binding signal was abolished in the κ-KO mice, as reflected by the lack of differential uptake in the striatum relative to cerebellum in KO versus WT mice (Fig. 4, right). Ligand concentration were 3.0 ± 0.6 ng/g in the striatum of WT mice and were 5 times lower, at 0.6 ± 0.2 ng/g, in the KO mice. Concentrations in the cerebellum were similar for WT (1.0 ± 0.6 ng/g) and KO mice (0.7 ± 0.2 ng/g). There was no significant difference between cerebellar levels in the KO and WT mice or between striatal and cerebellar levels in the KO mice. There was a significant difference in ligand concentrations between the striatum and cerebellum of WT mice (unpaired *t* test, $P < 0.05$) and between the striatum of WT and KO mice (unpaired *t* test, $P < 0.05$). These data indicate that binding of LY2795050 in the rodent brain is KOR-specific.

In terms of specific binding signals, LY2795050 performed similarly to GR103545, an agonist ligand evaluated previously by LC/MS/MS determination of ligand tissue distribution (*26,37*) and by PET experiments in baboons (*20*). GR103545 is a known PET tracer available for KOR imaging, but as an agonist it has the potential liability of causing psychotomimetic effects even at microdosing (μg) level (*38*), whereas an antagonist tracer will not have this liability and thus would provide a much wider safety margin. Results from these ex vivo determinations of tissue distribution indicate that LY2795050 has good brain uptake at 10 min, tissue kinetics appropriate for PET imaging with an ^{11}C-labeled radioligand, and a benzamide site amenable to ^{11}C radiolabeling with ^{11}C-cyanide under palladium-catalysis conditions, followed by partial hydrolysis. In addition, the specific binding of LY2795050 in the rat brain was blocked in a dose-dependent manner by a structurally similar KOR-selective antagonist (*26*). Hence, LY2795050 represents a potential tracer candidate able to provide measurable KOR-specific binding signals in vivo. On the basis of these findings, radiolabeling was performed, and the labeled compound, ^{11}C-LY2795050, was evaluated in nonhuman primates.

Radiochemistry

^{11}C-LY2795050 (**5**) was synthesized from the iodophenyl precursor **10** by reaction with ^{11}C-cyanide under Pd_2dba_3/dppf catalysis to provide the intermediate **12**, followed by partial hydrolysis of the cyano group to an amide (Fig. 2). Starting from the enantiomerically pure precursor (**10**), this 2-step radiosynthetic sequence provided ^{11}C-LY2795050 in greater than 99% radiochemical and enantiomeric purity, as indicated by HPLC analysis of the final product (Fig. 3, bottom). The average radiochemical yield was 12% at the end of synthesis (calculated from trapped ^{11}C-cyanide, decay-uncorrected), with an average specific activity of 23.68 GBq/μmol at the

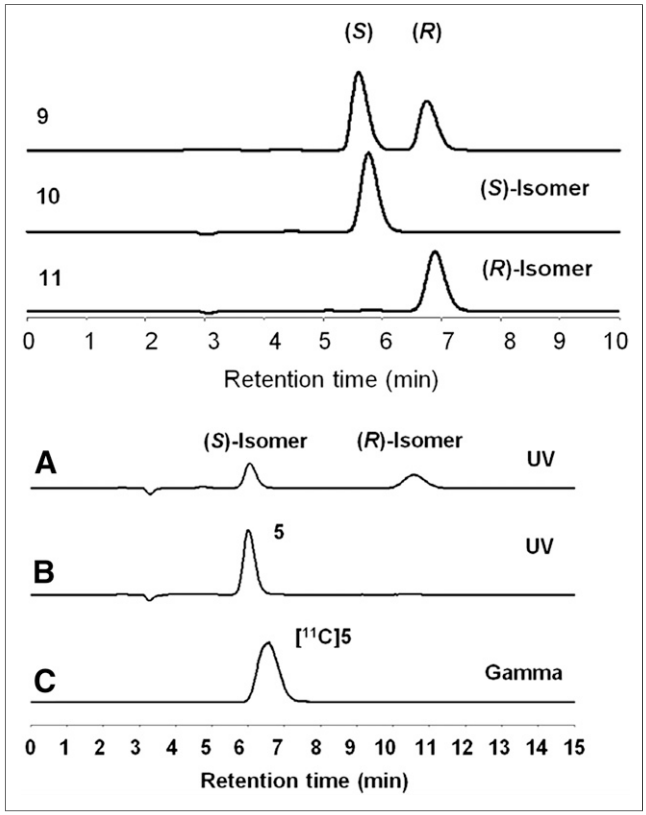

FIGURE 3. (Top) Analytic chiral HPLC profiles for compounds **9**, **10**, and **11**. Desired (*S*)-enantiomer (**10**) elutes first at 5.9 min, and undesired (*R*)-enantiomer (**11**) elutes later at 6.8 min. Conditions: Chiralpak AS-H column (4.6 × 150 mm) eluting with 0.2% Et_3N in MeOH at a flow rate of 0.85 mL/min. (Bottom) Analytic chiral HPLC chromatograms of labeled product ^{11}C-LY2795050. (A) UV trace for racemic counterpart of compound **5** with (*S*)-enantiomer (**5**) at retention time of 6.0 min and (*R*)-enantiomer at retention time of 10.6 min. (B and C) UV and γ-traces for ^{11}C-LY2795050. Conditions: Chiralpak AS-H column (4.6 × 150 mm) eluting with 0.2% Et_3N in MeOH at flow rate of 0.8 mL/min. UV = ultraviolet.

TABLE 1
In Vitro Binding Affinities and Functional Activities of LY2795050 at Cloned Human Opioid Receptors

Compound	K_i (nM)			Antagonist activity (K_b, nM)			Agonist activity (EC_{50}, nM)		
	κ	μ	δ	κ	μ	δ	κ	μ	δ
LY2795050	0.72	25.8	153	0.63	6.80	83.3	>10,000	>10,000	>10,000
Naltrexone	1.88	0.62	12.3	2.26	0.47	11.3	>10,000	>10,000	>10,000
JDTic	0.06	11.5	188	0.10	6.58	168	>10,000	>10,000	>10,000
GR103545	0.44	33.5	423	>1,400	17.7	>1,720	0.09	>10,000	34.7

Data presented are mean of 3 separate determinations.

end of synthesis (n = 16). Total synthesis time was about 45 min.

In Vivo Evaluation

After a bolus injection of ^{11}C-LY2795050 (mean injected activity, 133.2 MBq; mean injected mass, 4.1 μg), arterial blood samples were collected to measure the remaining fraction of parent tracer over time and calculate the metabolite-corrected plasma input function. At 30 min after tracer injection, the parent fraction was approximately 40%, indicating a moderate rate of metabolism for the radioligand. Radioactive metabolites were more polar than the parent ligand, as judged from the HPLC trace. The free fraction of the radioligand in the plasma was about 1%.

In the monkey brain, ^{11}C-LY2795050 displayed good uptake and a heterogeneous distribution pattern, with the highest levels of activity in the basal ganglia and cingulate cortex (Fig. 5, top). Naloxone (1 mg/kg) reduced the uptake of ^{11}C-LY2795050 in KOR-rich regions to the same level as that in the cerebellum (Fig. 5, middle). The selective κ-antagonist LY2456302 (**4**), at a dose of 96.0 μg/kg, also reduced significantly the uptake levels of ^{11}C-LY2795050 in KOR-rich brain regions (Fig. 5, bottom).

^{11}C-LY2795050 time–activity curves in various brain regions are presented in Figure 6. Uptake was higher in the globus pallidus and cingulate cortex; lower in the caudate, putamen, and frontal cortex; and lowest in the cerebellum (Fig. 6, left). Regional activity in the brain reached peak levels within 20 min of ^{11}C-LY2795050 injection, indicating fast uptake kinetics, a favorable property for a ^{11}C-labeled radiotracer. When the nonselective opioid antagonist naloxone was given before ^{11}C-LY2795050, regional activity levels were greatly reduced, and time–activity curves in higher-binding regions trended down to the same level as the cerebellum (Fig. 6, middle), demonstrating that binding of ^{11}C-LY2795050 is saturable and specific to the opioid receptor. Furthermore, regional binding of ^{11}C-LY2795050 was also reduced by treatment with the selective κ-antagonist LY2456302 (**4**). Uptake levels of ^{11}C-LY2795050 were lower when the monkey was treated with LY2456302 at a dose of 96 μg/kg (Fig. 6, right).

Time–activity curves were analyzed with 1TC and 2TC using the metabolite-corrected plasma time–activity curves as input functions. The 2TC provided better fits to the data than did the 1TC. Regional V_T values were therefore derived using the 2TC. Values of regional BP_{ND}, as a measure of specific binding signal, were calculated using cerebellum as the reference region and are listed in Table 2. Values derived from both 2TC and SRTM are presented. In the baseline scans, regional BP_{ND} values derived from 2TC followed the order of globus pallidus > cingulate cortex > insula > caudate > frontal cortex > temporal cortex. When the monkeys were pretreated with the nonselective opioid antagonist naloxone (1 mg/kg), specific binding signals were almost completely abolished, as reflected by the negligible BP_{ND} values. Further, specific binding of ^{11}C-LY2795050 was reduced in a dose-dependent manner (Fig. 7) when the monkey was treated with escalating doses of the selective KOR antagonist LY2456302 (**4**) (K_i = 0.95, 22.7, and 166 nM, respectively, for KOR, MOR, and DOR) (*26*). These results indicate that in the monkey brain, ^{11}C-LY2795050 binds to the KOR specifically and selectively and provides specific binding signals that can be reliably measured in most brain regions (regional BP_{ND} values > 0.5) (*39*).

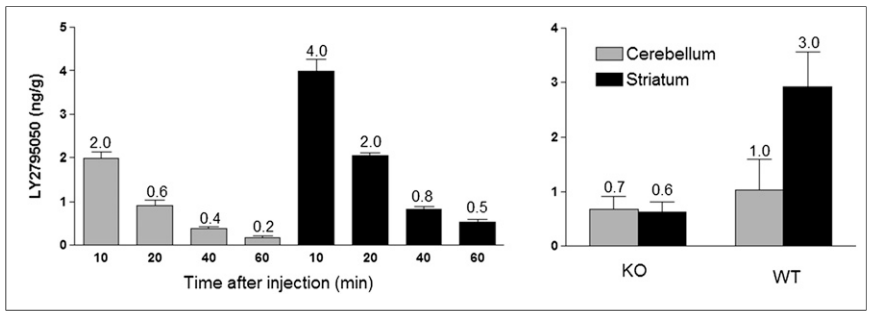

FIGURE 4. (Left) Ligand concentrations measured in striatum and cerebellum of Sprague–Dawley rats at 10, 20, 40, and 60 min (n = 4 rats per time point) after administration of LY2795050 (3 μg/g). (Right) Concentrations of LY2795050 in striatum and cerebellum, at 60 min after dosing (3 μg/g), in κ-KO (n = 8) and WT (n = 9) mice.

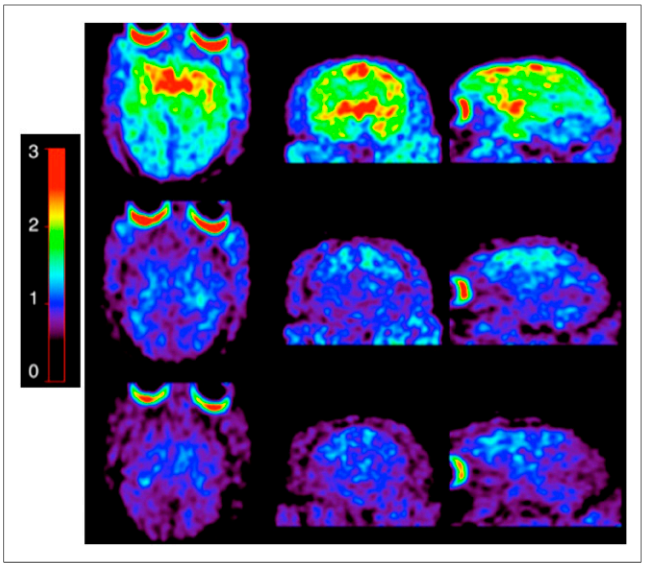

FIGURE 5. PET images of ^{11}C-LY2795050 in transverse (left), coronal (middle) and sagittal views (right). PET images are summed from 60 to 90 min after injection of ^{11}C-LY2795050. (Top) PET images from baseline scan with ^{11}C-LY2795050. (Middle) Images taken from naloxone (1 mg/kg) blocking scan. (Bottom) Images from blocking scan with LY2456302 (96 μg/kg). Activity level is presented as standardized uptake value unit, that is, radioactivity concentrations normalized by dose per kilogram of body weight.

DISCUSSION

We have previously reported the synthesis of a new series of selective KOR antagonists (*26*). Pharmacologic studies indicated that among these new compounds LY2795050 displays subnanomolar affinity to the cloned human KOR and greater than 35-fold selectivity over μ-and δ-receptor subtypes. Using a microdosing regimen with the unlabeled compound and LC/MS/MS determination of ligand concentrations in rat brain regions, we found that LY2795050 had higher levels in κ-rich striatum, with a striatum-to-cerebellum ratio of 3.3 at 60 min after dosing. Further experiments in WT and κ-KO mice indicated the absence of specific binding in the KO animals. Together, these results demonstrated the ability of LY2795050 to enter the brain and bind specifically to KOR.

The PET radioligand ^{11}C-LY2795050 was prepared in high radiochemical purity in a 2-step radiosynthetic pathway using ^{11}C-HCN as the radiolabeling agent. Imaging experiments in rhesus monkeys demonstrated that ^{11}C-LY2795050 binds to the brain KOR specifically and selectively. It presents a favorable metabolic profile and good regional specific binding signals. In comparison to ^{11}C-GR103545, a KOR agonist radiotracer previously evaluated in baboons (*20*), ^{11}C-LY2795050 possesses faster uptake kinetics, enabling the quantitative analysis of binding parameters with a shorter scan duration and thus is a favorable property for a ^{11}C-labeled tracer. On the other hand, specific binding signals, as measured by regional BP_{ND} values, are higher for ^{11}C-GR103545 than ^{11}C-LY2795050. For example, the BP_{ND} value in the cingulate cortex is 0.63 for ^{11}C-LY2795050 and 1.9 for ^{11}C-GR103545. The safety profile, however, favors ^{11}C-LY2795050. In baboon studies with ^{11}C-GR103545, because of the potent agonist effect of the tracer, injected mass was limited to 0.3 μg/kg. In the present study, up to 1 μg/kg of tracer mass and up to 313 μg/kg of the selective KOR antagonist LY2456302 were given without any observable effects for the monkeys. Taken together, ^{11}C-GR103545 and ^{11}C-LY2795050, as selective KOR agonist and antagonist tracers, respectively, have their separate characteristics and may both prove to be useful as PET agents for KOR in humans. A side-by-side comparison of these 2 radiotracers in humans will be needed to determine their respective merits as imaging agents to measure KOR in vivo.

CONCLUSION

We have successfully identified, synthesized, and evaluated ^{11}C-LY2795050 as the first selective antagonist for PET of KOR in monkeys. On the basis of its favorable characteristics, ^{11}C-LY2795050 has been advanced to eval-

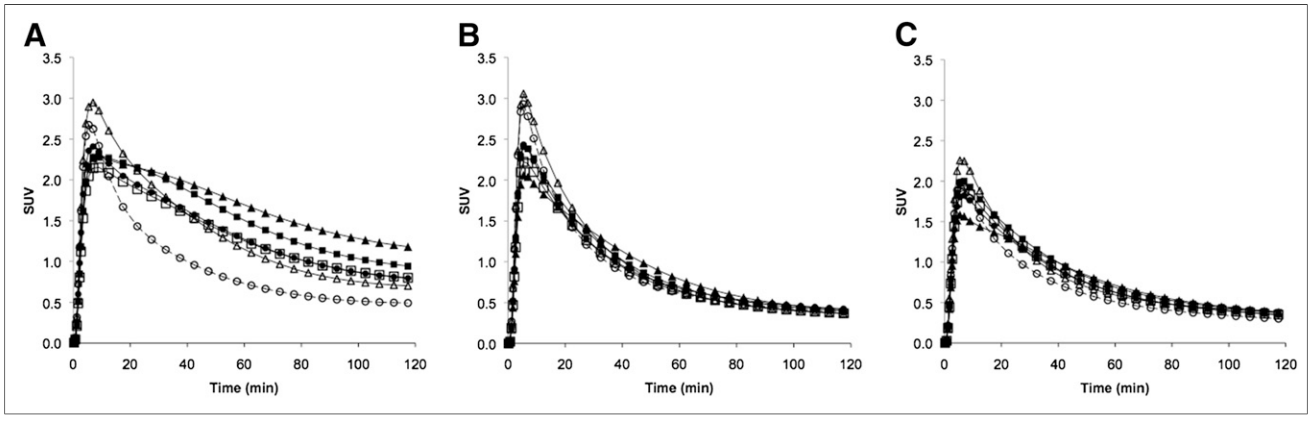

FIGURE 6. (A) Time–activity curves in monkey brain regions after administration of ^{11}C-LY2795050. Highest uptake at later time is in globus pallidus (▲), followed by cingulate cortex (■), frontal cortex (□), caudate (●), and putamen (Δ). Lowest uptake is in cerebellum (○). (B) Time–activity curves after ^{11}C-LY2795050 administration 10 min after naloxone (1 mg/kg). (C) Time–activity curves after coadministration of ^{11}C-LY2795050 and LY2456302 (96 μg/kg). SUV = standardized uptake value.

TABLE 2
Regional V_T and BP_{ND} of ^{11}C-LY2795050 Under Different Conditions

Condition	Dose	Globus pallidus	Putamen	Substantia nigra	Caudate	Cingulate cortex	Insula	Frontal cortex	Temporal cortex	Cerebellum
2T V_T										
Baseline (n = 4)	—	5.15 ± 1.37	4.17 ± 0.49	3.80 ± 1.35	3.01 ± 1.35	3.74 ± 1.37	3.40 ± 1.04	2.98 ± 1.08	2.82 ± 0.91	2.43 ± 0.63
Naloxone (n = 2)	1 mg/kg	2.44 ± 1.40	2.47 ± 1.29	3.33 ± 0.00	2.40 ± 1.43	2.45 ± 1.31	2. 20 ± 1.20	2.18 ± 1.32	2.17 ± 1.26	2.40 ± 1.22
2T BP_{ND}										
Baseline (n = 4)	—	0.97 ± 0.10	0.66 ± 0.25	0.58 ± 0.16	0.32 ± 0.26	0.63 ± 0.21	0.39 ± 0.17	0.30 ± 0.16	0.15 ± 0.12	—
Naloxone (n = 2)	1 mg/kg	0.00 ± 0.07	0.03 ± 0.02	0.02 ± 0.00	−0.02 ± 0.10	0.02 ± 0.03	−0.09 ± 0.04	−0.12 ± 0.10	−0.11 ± 0.07	—
SRTM BP_{ND}										
Baseline (n = 4)	—	0.84 ± 0.23	0.65 ± 0.18	0.78 ± 0.36	0.43 ± 0.07	0.66 ± 0.15	0.44 ± 0.11	0.33 ± 0.11	0.18 ± 0.07	—
Naloxone (n = 2)	1 mg/kg	0.06 ± 0.05	0.06 ± 0.08	−0.02 ± 0.00	0.02 ± 0.01	0.05 ± 0.00	−0.02 ± 0.01	−0.06 ± 0.04	−0.07 ± 0.03	—

Data are mean ± SD.

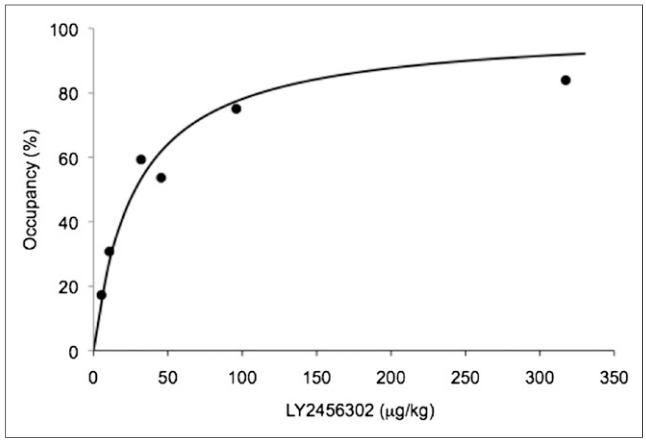

FIGURE 7. Blockade of ^{11}C-LY2795050 binding by varying doses of LY2456302 measured from blocking experiments in 2 monkeys demonstrates that specific binding of ^{11}C-LY279505 is displaceable by selective KOR antagonist. KOR occupancy (%) is derived from occupancy plot (*35*). ID_{50} value for LY245302—that is, dose of LY2456302 to inhibit 50% of ^{11}C-LY2795050 binding—is estimated at 28.1 μg/kg.

uation and PET applications in humans. Preliminary results indicated that the in vivo pharmacokinetic and specific binding properties of ^{11}C-LY2795050 described here in nonhuman primates translated well into humans, and the radiotracer can be used to reliably quantitate KOR in the human brain (*40*). A full report on the characterization of this radiotracer in humans will be presented in due course.

DISCLOSURE

The costs of publication of this article were defrayed in part by the payment of page charges. Therefore, and solely to indicate this fact, this article is hereby marked "advertisement" in accordance with 18 USC section 1734. This project was supported by a research contract from Eli Lilly & Co. This publication was also made possible by CTSA grant UL1 RR024139 from the National Center for Research Resources (NCRR) and the National Center for Advancing Translational Science (NCATS), components of the National Institutes of Health (NIH), and NIH roadmap for medical research. Its contents are solely the responsibility of the authors and do not necessarily represent the official view of NIH. No other potential conflict of interest relevant to this article was reported.

ACKNOWLEDGMENTS

We thank the staff at the Yale PET Center for their expert assistance.

REFERENCES

1. Dhawan BN, Cesselin F, Raghubir R, et al. International Union of Pharmacology. XII. Classification of opioid receptors. *Pharmacol Rev.* 1996;48:567–592.
2. Minami M, Satoh M. Molecular biology of the opioid receptors: structures, functions and distributions. *Neurosci Res.* 1995;23:121–145.
3. Brady LS, Herkenham M, Rothman RB, et al. Region-specific up-regulation of opioid receptor binding in enkephalin knockout mice. *Brain Res Mol Brain Res.* 1999;68:193–197.

4. Mansour A, Khachaturian H, Lewis ME, Akil H, Watson SJ. Autoradiographic differentiation of mu, delta, and kappa opioid receptors in the rat forebrain and midbrain. *J Neurosci.* 1987;7:2445–2464.
5. Slowe SJ, Simonin F, Kieffer B, Kitchen I. Quantitative autoradiography of mu-, delta- and kappa1 opioid receptors in kappa-opioid receptor knockout mice. *Brain Res.* 1999;818:335–345.
6. Nock B, Rajpara A, O'Connor LH, Cicero TJ. Autoradiography of [^{3}H]U-69593 binding sites in rat brain: evidence for kappa opioid receptor subtypes. *Eur J Pharmacol.* 1988;154:27–34.
7. Unterwald EM, Knapp C, Zukin RS. Neuroanatomical localization of kappa 1 and kappa 2 opioid receptors in rat and guinea pig brain. *Brain Res.* 1991;562:57–65.
8. Hiller JM, Fan LQ. Laminar distribution of the multiple opioid receptors in the human cerebral cortex. *Neurochem Res.* 1996;21:1333–1345.
9. Mathieu-Kia AM, Fan LQ, Kreek MJ, Simon EJ, Hiller JM. Mu-, delta- and kappa-opioid receptor populations are differentially altered in distinct areas of postmortem brains of Alzheimer's disease patients. *Brain Res.* 2001;893:121–134.
10. Peckys D, Landwehrmeyer GB. Expression of mu, kappa, and delta opioid receptor messenger RNA in the human CNS: a 33P in situ hybridization study. *Neuroscience.* 1999;88:1093–1135.
11. Simonin F, Gaveriaux-Ruff C, Befort K, et al. kappa-Opioid receptor in humans: cDNA and genomic cloning, chromosomal assignment, functional expression, pharmacology, and expression pattern in the central nervous system. *Proc Natl Acad Sci USA.* 1995;92:7006–7010.
12. Ko MC, Lee H, Harrison C, et al. Studies of micro-, kappa-, and delta-opioid receptor density and G protein activation in the cortex and thalamus of monkeys. *J Pharmacol Exp Ther.* 2003;306:179–186.
13. Slater P, Cross AJ. Autoradiographic distribution of dynorphin1-9 binding sites in primate brain. *Neuropeptides.* 1986;8:71–76.
14. Tejeda HA, Shippenberg TS, Henriksen R. The dynorphin/k-opioid receptor system and its role in psychiatric disorders. *Cell Mol Life Sci.* 2012;69:857–896.
15. Henriksen G, Willoch F. Imaging of opioid receptors in the central nervous system. *Brain.* 2008;131:1171–1196.
16. Chesis PL, Welch MJ. Synthesis and in vitro characterization of fluorinated U-50488 analogs for PET studies of kappa opioid receptors. *Int J Rad Appl Instrum [A].* 1990;41:267–273.
17. Noble G, Dannals RF, Ravert HT, Wilson AA, Wagner HN. Synthesis of a radiotracer for studying k-subtype opiate receptors: *N*-[^{11}C-methyl]-*N*-(*trans*-2-pyrrolidinyl-cyclohexyl)-3,4-dichlorophenylacetamide ([^{11}C]-(±)-U-50488H). *J Labelled Comp Radiopharm.* 1992;31:81–89.
18. Ravert HT, Mathews WB, Musachio JL, Scheffel U, Finley P, Dannals RF. [^{11}C]-methyl 4-[(3,4-dichlorophenyl)acetyl]-3-[(1-pyrrolidinyl)-methyl]-1-piperazine-carboxylate ([^{11}C]GR89696): synthesis and in vivo binding to kappa opiate receptors. *Nucl Med Biol.* 1999;26:737–741.
19. Ravert HT, Scheffel U, Mathews WB, Musachio JL, Dannals RF. [^{11}C]-GR89696, a potent kappa opiate receptor radioligand; in vivo binding of the *R* and *S* enantiomers. *Nucl Med Biol.* 2002;29:47–53.
20. Talbot PS, Narendran R, Butelman ER, et al. ^{11}C-GR103545, a radiotracer for imaging kappa-opioid receptors in vivo with PET: synthesis and evaluation in baboons. *J Nucl Med.* 2005;46:484–494.
21. Tomasi G, Zheng M-Q, Weinzimmer D, et al. Kinetic modeling of the kappa agonist tracer [^{11}C]GR103545 in humans [abstract]. *J Nucl Med*. 2010;51:1293p.
22. Schoultz BW, Arstad E, Marton J, et al. A new method for radiosynthesis of ^{11}C-labeled carbamate groups and its application for a highly efficient synthesis of the kappa-opioid receptor tracer [^{11}C]GR103545. *Open Med Chem J.* 2008;2:72–74.
23. Wilson AA, Garcia A, Houle S, Vasdev N. Direct fixation of [^{11}C]CO_2 by amines: formation of [^{11}C-carbonyl]-methylcarbamates. *Org Biomol Chem.* 2010;8:428–432.
24. Nabulsi NB, Zheng MQ, Ropchan J, et al. [^{11}C]GR103545: novel one-pot radiosynthesis with high specific activity. *Nucl Med Biol.* 2011;38:215–221.
25. Poisnel G, Oueslati F, Dhilly M, et al. [^{11}C]-MeJDTic: a novel radioligand for kappa-opioid receptor positron emission tomography imaging. *Nucl Med Biol.* 2008;35:561–569.
26. Mitch CH, Quimby SJ, Diaz N, et al. Discovery of aminobenzyloxyarylamides as kappa opioid receptor selective antagonists: application to preclinical development of a kappa opioid receptor antagonist receptor occupancy tracer. *J Med Chem.* 2011;54:8000–8012.
27. Ansonoff MA, Zhang J, Czyzyk T, et al. Antinociceptive and hypothermic effects of Salvinorin A are abolished in a novel strain of kappa-opioid receptor-1 knockout mice. *J Pharmacol Exp Ther.* 2006;318:641–648.
28. Chefer VI, Czyzyk T, Bolan EA, Moron J, Pintar JE, Shippenberg TS. Endogenous kappa-opioid receptor systems regulate mesoaccumbal dopamine dynamics and vulnerability to cocaine. *J Neurosci.* 2005;25:5029–5037.
29. Czyzyk TA, Nogueiras R, Lockwood JF, et al. Kappa-opioid receptors control the metabolic response to a high-energy diet in mice. *FASEB J.* 2010;24:1151–1159.
30. Mansour A, Fox CA, Burke S, et al. Mu, delta, and kappa opioid receptor mRNA expression in the rat CNS: an in situ hybridization study. *J Comp Neurol.* 1994;350:412–438.
31. Nabulsi N, Huang Y, Weinzimmer D, et al. High-resolution imaging of brain 5-HT 1B receptors in the rhesus monkey using [^{11}C]P943. *Nucl Med Biol.* 2010;37:205–214.
32. Hilton J, Yokoi F, Dannals RF, Ravert HT, Szabo Z, Wong DF. Column-switching HPLC for the analysis of plasma in PET imaging studies. *Nucl Med Biol.* 2000;27:627–630.
33. Innis RB, Cunningham VJ, Delforge J, et al. Consensus nomenclature for in vivo imaging of reversibly binding radioligands. *J Cereb Blood Flow Metab.* 2007;27:1533–1539.
34. Lammertsma AA, Hume SP. Simplified reference tissue model for PET receptor studies. *Neuroimage.* 1996;4:153–158.
35. Cunningham VJ, Rabiner EA, Slifstein M, Laruelle M, Gunn RN. Measuring drug occupancy in the absence of a reference region: the Lassen plot re-visited. *J Cereb Blood Flow Metab.* 2010;30:46–50.
36. Chernet E, Martin LJ, Li D, et al. Use of LC/MS to assess brain tracer distribution in preclinical, in vivo receptor occupancy studies: Dopamine D_2, serotonin 2A and NK-1 receptors as examples. *Life Sci.* 2005;78:340–346.
37. Need AB, McKinzie JH, Mitch CH, Statnick MA, Phebus LA. In vivo rat brain opioid receptor binding of LY255582 assessed with a novel method using LC/MS/MS and the administration of three tracers simultaneously. *Life Sci.* 2007;81:1389–1396.
38. Pfeiffer A, Brantl V, Herz A, Emrich HM. Psychotomimesis mediated by kappa opiate receptors. *Science.* 1986;233:774–776.
39. Laruelle M, Slifstein M, Huang Y. Relationships between radiotracer properties and image quality in molecular imaging of the brain with positron emission tomography. *Mol Imaging Biol.* 2003;5:363–375.
40. Huang Y, Williams W, Tomasi G, et al. Imaging kappa opioid receptor in humans with a novel antagonist tracer, [^{11}C]LY2795050 [abstract]. *J Nucl Med.* 2010;51:102p.

The Journal of NUCLEAR MEDICINE

Synthesis and Evaluation of ^{11}C-LY2795050 as a κ-Opioid Receptor Antagonist Radiotracer for PET Imaging

Ming-Qiang Zheng, Nabeel Nabulsi, Su Jin Kim, Giampaolo Tomasi, Shu-fei Lin, Charles Mitch, Steven Quimby, Vanessa Barth, Karen Rash, John Masters, Antonio Navarro, Eric Seest, Evan D. Morris, Richard E. Carson and Yiyun Huang

J Nucl Med. 2013;54:455-463.
Published online: January 25, 2013.
Doi: 10.2967/jnumed.112.109512

The Journal of Nuclear Medicine is published monthly.
SNMMI | Society of Nuclear Medicine and Molecular Imaging
1850 Samuel Morse Drive, Reston, VA 20190.
(Print ISSN: 0161-5505, Online ISSN: 2159-662X)

SNMMI SOCIETY OF NUCLEAR MEDICINE AND MOLECULAR IMAGING